The unintended victims of rat poison p. 134

Mapping Neanderthal-human gene flow pp. 132 & 158

Engineering electrons with chirality p. 183

Science

$15
12 JULY 2024
science.org

AAAS

STEALTH FUNGUS

White-nose pathogen evades bat skin defenses pp. 142 & 194

FUNGAL PATHOGENS

Pathogenic strategies of *Pseudogymnoascus destructans* during torpor and arousal of hibernating bats

Marcos Isidoro-Ayza and Bruce S. Klein*

Millions of hibernating bats across North America have died from white-nose syndrome (WNS), an emerging disease caused by a psychrophilic (cold-loving) fungus, *Pseudogymnoascus destructans*, that invades their skin. Mechanisms of *P. destructans* invasion of bat epidermis remain obscure. Guided by our in vivo observations, we modeled hibernation with a newly generated little brown bat (*Myotis lucifugus*) keratinocyte cell line. We uncovered the stealth intracellular lifestyle of *P. destructans*, which inhibits apoptosis of keratinocytes and spreads through the cells by two epidermal growth factor receptor (EGFR)–dependent mechanisms: active penetration during torpor and induced endocytosis during arousal. Melanin of endocytosed *P. destructans* blocks endolysosomal maturation, facilitating *P. destructans* survival and germination after return to torpor. Blockade of EGFR aborts *P. destructans* entry into keratinocytes.

Bats sustain our planet's biodiversity and ecosystems, enhancing human, animal, and economic health (*1*, *2*). White-nose syndrome (WNS) is among the most pressing threats for hibernating bats in the US and Canada (*3*). Since the first report in 2007, WNS has killed millions of North American bats, with >95% decline in some species and extirpation of entire populations (*3*–*5*). The once ubiquitous and now endangered little brown bat (*Myotis lucifugus*) is one of the most susceptible species (*3*–*8*). *Pseudogymnoascus destructans*, the causative agent of WNS, is a psychrophilic (cold-loving) ascomycete fungus (*6*, *8*). Without bats, *P. destructans* survives in caves and mines as dormant conidia (*5*). During hibernation, *P. destructans* primarily infects the skin of the wing and tail membranes (patagia) of bats that perform vital regulatory functions, leading to physiological effects that arouse them frequently, consume their limited fat stores, and cause them to die from starvation (*5*, *8*).

The urgent need to prevent the spread of WNS and mitigate the impacts of this disease on susceptible bat species has prompted calls to develop treatment and prevention strategies. However, these developments are hindered by a lack of knowledge about the mechanisms that underlie the early stages of *P. destructans* invasion of the bat epidermis. In this work, we present evidence of *P. destructans* entry into epidermal keratinocytes of little brown bats during early WNS by two epidermal growth factor receptor (EGFR)–mediated mechanisms influenced by the host's physiological state: torpor or arousal.

Department of Pediatrics, Medicine and Medical Microbiology and Immunology, School of Medicine and Public Health, University of Wisconsin–Madison, Madison, WI 53706, USA.
***Corresponding author. Email: bsklein@wisc.edu**

Results

Ultrastructure of early P. destructans–bat interaction

P. destructans colonizes the skin of bats by invading the epidermis (Fig. 1A) (*5*, *6*, *8*). We have examined the patagia of little brown bats with WNS by electron microscopy (EM) and focused our investigations on areas with a light *P. destructans* burden, where the skin architecture has not been substantially disrupted. These areas are representative of the early stages of *P. destructans* invasion, where pathogen-host interactions can be better discerned (Fig. 1A). We observed that *P. destructans* hyphae adhered to the skin surface, progressing between terminally differentiated keratinocytes of the stratum corneum (corneocytes) (Fig. 1B). These hyphae also reached deeper into the noncornified epidermis formed by one to two layers of live keratinocytes (Fig. 1B) (*9*). We observed hyphae inside apparently viable keratinocytes and surrounded by a cell membrane (intracellular but extracytosolic) (Fig. 1, B and C). Moreover, we found conidia associated with keratinocytes in superficial and deeper epidermal strata (Fig. 1D).

Modeling early P. destructans skin invasion

To identify mechanisms of early *P. destructans* invasion into bat keratinocytes, we established an in vitro cellular model of hibernation mimicking intervals of torpor and arousal. We created a little brown bat keratinocyte cell line (Myluk) by isolating primary keratinocytes and integrating HPV-16 oncogenes E6 and E7 through a lentiviral vector to immortalize the cell line (*10*) (fig. S1A). We cloned the Myluk keratinocytes and showed that they grow in a cobblestone pattern as a monolayer and express cytokeratins (Fig. 1E). During hibernation, bats undergo multiple cycles of torpor (cold phase) followed by arousals (warm phase). *P. destructans* germinates and grows optimally at 12° to 16°C, a temperature favoring torpor, whereas bat cell metabolic activity peaks u arousal at 37°C (*5*, *11*, *12*). Thus, we confir that Myluk cells resist cold stress, as do cells of other hibernating mammals (*13*) (fig. S1B), and undergo metabolic activation upon transition from 12° to 37°C (fig. S1C and data S2). Given these results, we established a two-phase in vitro infection model resembling torpor and arousal in hibernating bats (Fig. 1F). Briefly, we grew keratinocytes to confluence at 37°C, differentiated them overnight by increasing Ca^{2+} concentration, introduced ungerminated live *P. destructans* conidia into the culture, and incubated the combined culture for 1 to 2 days at 12°C to mimic the torpor phase of bat hibernation. We brought the cultures back to 37°C for 4 to 8 hours to mimic the arousal phase and allow metabolic reactivation of the keratinocytes.

Hibernation model recapitulates in vivo observations of early P. destructans invasion of keratinocytes

We analyzed cocultures of *P. destructans* with Myluk cells by using scanning and transmission EM (SEM and TEM) and confocal microscopy. *P. destructans* hyphae and conidia were often observed inside keratinocytes (Fig. 1, G to L): 46 ± 19% of hyphae and 47 ± 6% of conidia were seen inside Myluk cells. Invasion rates were similar when we used primary keratinocytes from little brown bats or when we lowered the incubation temperature of the "warm phase" to 27°C, which is the average arousal skin temperature for free-ranging little brown bats (*14*) (figs. S2, A and B). Hyphae invaded keratinocytes, forming early invasion pockets (Fig. 1H), and progressed through multiple epithelial cells by forming transcellular tunnels without apparently breaching the plasma membrane (Fig. 1, I and J). Hyphae appeared to form the tunnels by exiting the first invaded cell upon fusion of the fungus-containing cell membrane with the plasma membrane and then invading the next cell (Fig. 1I), or they formed tunnels without exiting the first cell, remaining enveloped by its plasma membrane and cytoplasm, and forming an invagination into the contiguous keratinocyte (Fig. 1J). Conidia were often observed partially surrounded by keratinocyte pseudopodia (Fig. 1K) or internalized within tight lipid vesicles (Fig. 1L and fig. S3).

P. destructans–infected keratinocytes remain viable

Similar to our in vivo EM findings, neither hyphal nor conidial invasion of Myluk cells in vitro produced ultrastructural features of host cell death, such as vacuolation, karyorrhexis, or blebbing. To confirm these findings, we assayed viability of Myluk and primary keratinocytes from little brown bats challenged with live *P. destructans* conidia for up to 2 days by using propidium iodide (PI) staining and

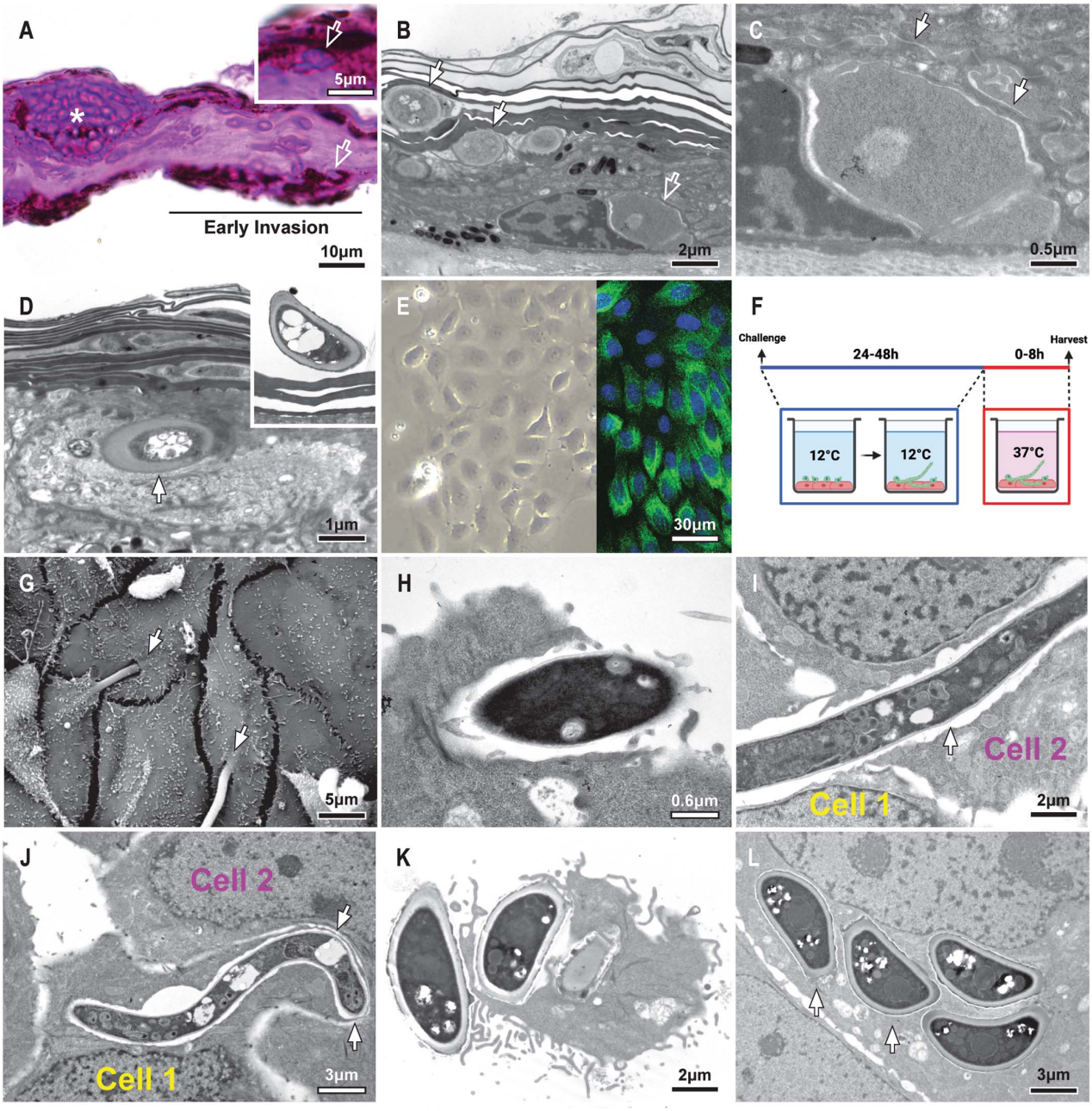

Fig. 1. Interaction of *P. destructans* with bat keratinocytes during early WNS. (**A**) Histological section (Periodic Acid Schiff stain) of the wing membrane (patagium) of a little brown bat (*M. lucifugus*) with WNS. *P. destructans* (bright magenta) invades the epidermis and breaches the epidermal barrier into the dermis. The asterisk indicates an area of "advanced invasion," where a large cluster of *P. destructans* disrupts the epidermal architecture, forming a "cupping lesion." An area of "early invasion" with visible *P. destructans*–keratinocyte interactions is underscored. (Inset) *P. destructans* is shown within noncornified epidermis. The arrows point to *P. destructans* in close contact with or within keratinocytes (brown-pigmented cells). (**B** to **D**) TEM of an early invasion site in the epidermis of a little brown bat with WNS. (B) Extracellular *P. destructans* hyphae in the stratum corneum (white arrows) and intracellular *P. destructans* hypha in a viable keratinocyte (empty arrow). (C) Higher-magnification image with details of the intracellular, thin-walled, septate *P. destructans* hypha from (B). Arrow shows the keratinocyte plasma membrane, denoting cell boundaries. (D) A thick-walled conidia-like fungal structure located in the noncornified epidermis (arrow). (Inset) A conidia-like fungal form on the stratum corneum (skin surface) (**E**) (Left) Bright-field micrograph of the Myluk cell line. (Right) Confocal microscopy immunostaining with anti–pan-cytokeratin antibody (green) and 4′,6-diamidino-2-phenylindole nuclear counterstaining (blue). (**F**) Illustration of in vitro challenge of Myluk cells with *P. destructans* using the biphasic incubation model. (**G** to **L**) SEM (G) and TEM [(H) to (L)] of Myluk cells challenged with *P. destructans* using the biphasic incubation model (2 days at 12°C and 4 hours at 37°C). (G) Hyphal invasion sites of apparently viable keratinocytes (arrows). (H) Early hyphal invasion pocket. The hyphal tip enters a Myluk cell without disrupting the plasma membrane. (I) The arrow points at a *P. destructans* hypha invading two neighboring keratinocytes through a transcellular tunnel without disrupting the plasma membrane. The plasma and cell membranes of the intracellular compartment that contains the hypha are fused. (J) A *P. destructans* hypha invades two keratinocytes through a transcellular tunnel. The arrows point to the intact cytoplasm and plasma membrane of the first keratinocyte pushed by the hypha into the subsequent keratinocyte. (K) Myluk keratinocyte using pseudopodia to endocytose *P. destructans* conidia. (L) Arrows denote endocytosed conidia inside tight endocytic vesicles in a Myluk cell.

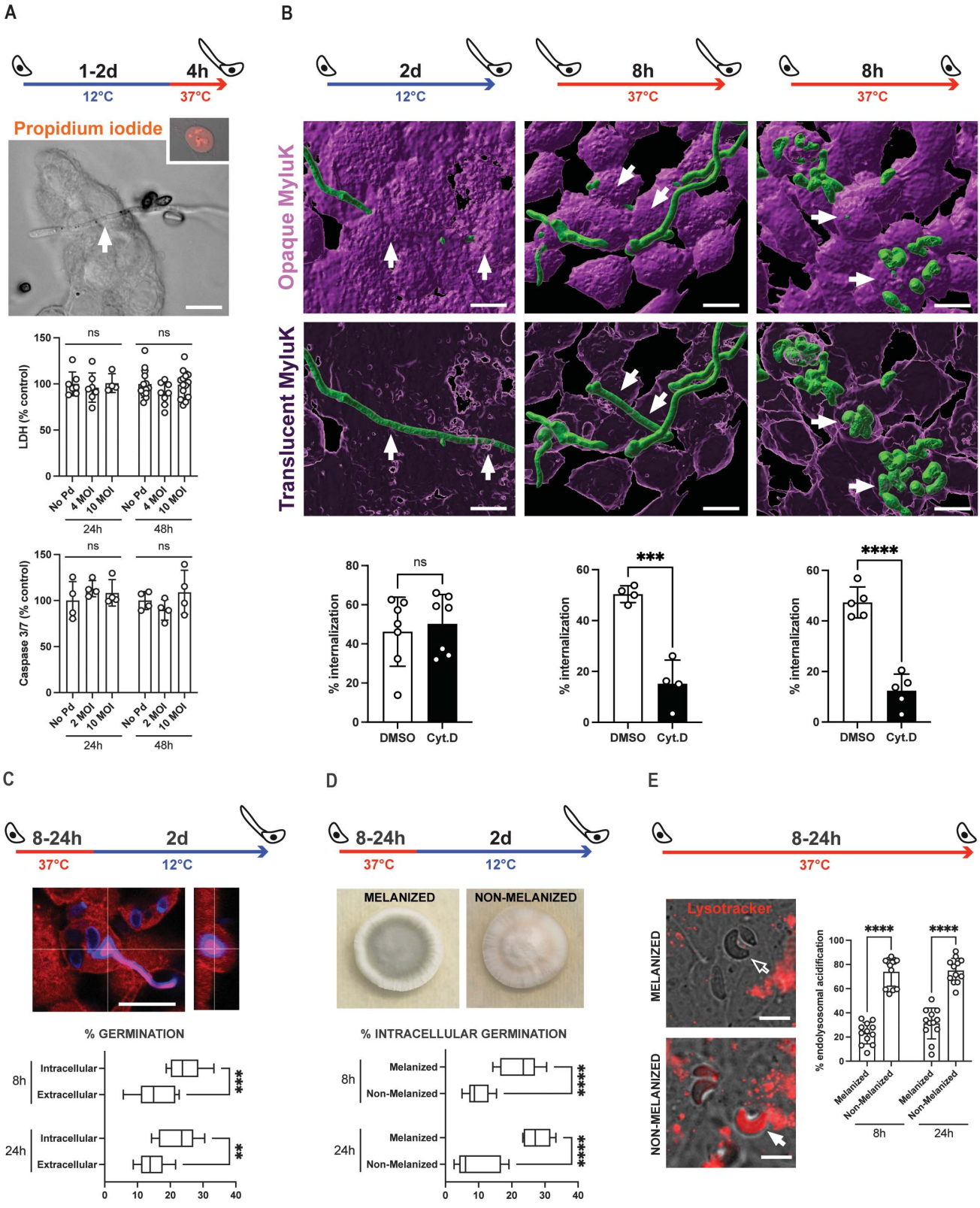

Fig. 2. Intracellular lifestyle of *P. destructans*. (**A**) Myluk cell viability assessment after challenge with *P. destructans*. Representative micrograph of merged DIC and confocal red channel of viable Myluk cells invaded by a *P. destructans* hypha (arrow) and incubated with PI viability stain. (Inset) Positive control cell treated with 0.1% Triton X-100 detergent for 20 min before PI staining. Graphs show quantification of LDH activity in supernatants and caspase 3 and 7 activity in Myluk cells. MOI, multiplicity of infection; no Pd, no *P. desctructans*. ns, not significant ($P > 0.05$). Two-way analysis of variance (ANOVA) with multiple comparisons correction. Scale bar, 20 µm. (**B** to **D**) Confocal images and quantification. Actin filaments of Myluk were stained with phalloidin-AF555

(red, pseudocolored pink), and chitin in *P. destructans* cell walls was stained with calcofluor white (blue, pseudocolored green). ****$P \leq 0.0001$; *** $P \leq 0.001$; ** $P \leq 0.01$; ns, not significant ($P > 0.05$). Student's *t* test (B) and two-way ANOVA with multiple comparisons correction [(C) and (D)]. Scale bars, 20 μm. (B) Representative images and quantification of hyphal and conidial entry into Myluk cells incubated at 12° or 37°C in the presence or absence of cytochalasin D (Cyt.D). (C) Representative confocal image of intracellularly germinated conidia and quantification of extracellular versus intracellular conidia germination rates. (D) Melanized (untreated) and nonmelanized (treated with 20 μg/mL of pyroquilon) *P. destructans* colonies and quantification of intracellular germination of melanized versus nonmelanized conidia. (**E**) Representative live images and quantification of percentage of endolysosomal acidification of merged phase contrast and epifluorescent red channel (acidic compartments) of LysoTracker™-stained Myluk cells containing internalized melanized and nonmelanized *P. destructans* conidia that exclude calcofluor white (blue, extracellular; none shown). The white arrow points at a fully acidified conidia-containing endolysosome. The empty arrow points at a nonacidified conidia-containing endosome. ****$P \leq 0.0001$. Two-way ANOVA with multiple comparisons correction. Scale bars, 5 μm.

lactate dehydrogenase (LDH) quantification. Infected keratinocytes excluded PI stain and showed no significant increase in LDH concentration in the supernatants compared with that of unchallenged cells (Fig. 2A and fig. S2C). We further investigated cell viability by measuring the activity of effector caspases 3 and 7 (apoptosis) and found no significant differences between challenged and unchallenged keratinocytes after 1 and 2 days of infection (Fig. 2A). Our results support a model during the early stages of the infection in which *P. destructans* propagates intracellularly through the skin epithelium of bats, causing minimal cell damage. This behavior resembles the biotrophic strategy of fungal pathogens of plants (*15*, *16*) and the invasive commensalism of other animal fungal pathogens, including *Aspergillus fumigatus* and *Candida albicans* during early epithelial infection, before they secrete the cytotoxins gliotoxin and candidalysin, respectively, and tissue damage ensues (*17*–*19*).

P. destructans mechanisms of cell entry

C. albicans and *A. fumigatus* enter host cells by active penetration (pathogen driven) or by induced endocytosis (host mediated) (*20*). We quantified cell entry by *P. destructans* conidia and hyphae with confocal microscopy to determine whether *P. destructans* uses either of these mechanisms to invade keratinocytes during torpor or arousal. We studied cold and warm conditions in the presence or absence of cytochalasin D, which inhibits actin polymerization (Fig. 2B and fig. S4). During infection for 2 days at 12°C, *P. destructans* hyphae entered keratinocytes by active penetration, as pretreatment with cytochalasin D did not retard cell entry. Conversely, during infection for 8 hours at 37°C, hyphae and conidia were internalized by induced endocytosis, as cytochalasin D treatment blocked *P. destructans* uptake. Thus, *P. destructans* uses different infection strategies depending on the life history phase of its host, i.e., active penetration during torpor and induced endocytosis upon arousal.

Melanin facilitates intracellular survival of P. destructans conidia

Keratinocytes are endocytic cells that form endolysosomes and kill invading skin microbes (*21*–*23*). However, resting *P. destructans* conidia germinate efficiently within bat keratinocytes as the temperature falls during torpor. When we reduced the temperature of coculture to 12°C for 2 days, 24.5 ± 5% of endocytosed conidia germinated and invaded neighboring keratinocytes, as measured by confocal microscopy (Fig. 2C). This germination rate was significantly higher than the rate for extracellular *P. destructans* conidia (Fig. 2C). This finding indicates that *P. destructans* conidia may interfere with key endocytic mechanisms of microbial degradation. In *A. fumigatus,* conidial cell wall 1,8-dihydroxynaphthalene (DHN)–melanin blocks phagolysosomal maturation in macrophages and neutrophils (*24*–*26*). Similar to *A. fumigatus* conidia, *P. destructans* conidia are pigmented green-gray, indicating the presence of DHN-melanin (Fig. 2D) (*27*). Moreover, we found that during coculture with Myluk cells, *P. destructans* also expresses the DHN-biosynthetic gene ortholog of hydroxynaphthalene reductase ARP2 (VC83_03697, 70.5% identity) (fig. S5) (*27*). We generated nonmelanized *P. destructans* conidia by growing *P. destructans* in the presence of the ARP2 inhibitor pyroquilon, confirming that DHN-melanin is responsible for their pigmentation (Fig. 2D).

We tested whether DHN-melanin in *P. destructans* conidia promotes intracellular survival and subsequent germination. We challenged Myluk cells at 37°C with melanized (untreated) or nonmelanized (treated with pyroquilon) conidia for 8 and 24 hours, then lowered the temperature of the cultures to 12°C for two days and quantified intracellular germination (Fig. 2D). The intracellular germination rate of nonmelanized conidia was reduced by 65.2% at 8 hours and 57.4% at 24 hours compared with the respective rates for melanized conidia (Fig. 2D). We used viability staining to quantify the survival of intracellular conidia after incubation with Myluk for 24 hours at 37°C and found that the viability of nonmelanized conidia was also significantly lower than that of melanized conidia (fig. S6A). Neither the extracellular germination rate nor the uptake into Myluk cells differed between melanized and nonmelanized conidia (fig. S6, B and C). Thus, melanin enables *P. destructans* to survive and germinate once the fungus enters the intracellular locale of keratinocytes.

We tested the hypothesis that conidial DHN-melanin promotes intracellular survival and germination of *P. destructans* by inhibiting keratinocyte endolysosomal maturation. We used Lysotracker™ staining and live imaging to quantify acidified conidia-containing endocytic vesicles (i.e., mature endolysosomes) after incubating conidia with keratinocytes at 37°C (Fig. 2E). Only 23 ± 9% and 31 ± 13% of the vesicles containing melanized *P. destructans* conidia became acidified after 8 and 24 hours of incubation, respectively (Fig. 2E). By contrast, the acidification rates rose by 3.2- and 2.4-fold, respectively, at these time points for vesicles containing the nonmelanized conidia (Fig. 2E). These results indicate that during bat arousals, DHN-melanin in the cell wall of dormant *P. destructans* conidia blocks endolysosomal maturation, enabling survival and subsequent conidial germination on return to the temperature that induces host torpor.

Analysis of RNA sequencing during pathogenesis to identify druggable targets

We investigated the transcriptional response of Myluk cells to *P. destructans* in our cellular torpor-arousal hibernation model. Canonical signaling pathways were enriched in *P. destructans*–challenged keratinocytes after rewarming the cells for 4 and 8 hours compared with their unchallenged controls (Fig. 3A). Consistent with endocytic internalization of *P. destructans* at 37°C, phagosome formation and other elements of endocytic processes were revealed to be activated after rewarming, including actin polymerization, and Rac and Rho guanosine triphosphatase pathways (*28*, *29*). Our transcriptomic analysis also showed activation of pathways regulated by the transmembrane tyrosine kinase, EGFR (Fig. 3A). EGFR also was highlighted as a regulatory gene, and known EGFR target genes were differentially expressed across all time points studied (Fig. 3B). Conversely, apoptosis pathways were found to be repressed, as exemplified by the up-regulation of genes encoding inhibitor of apoptosis proteins BIRC2, BIRC3, and BIRC4 (data S1). No pathways were enriched during the cold phase of infection (0 hours). Consistent with prior in vivo transcriptomic studies conducted on the wing skin of little brown bats with WNS (*12*, *30*, *31*), Myluk cells evinced an antifungal immune

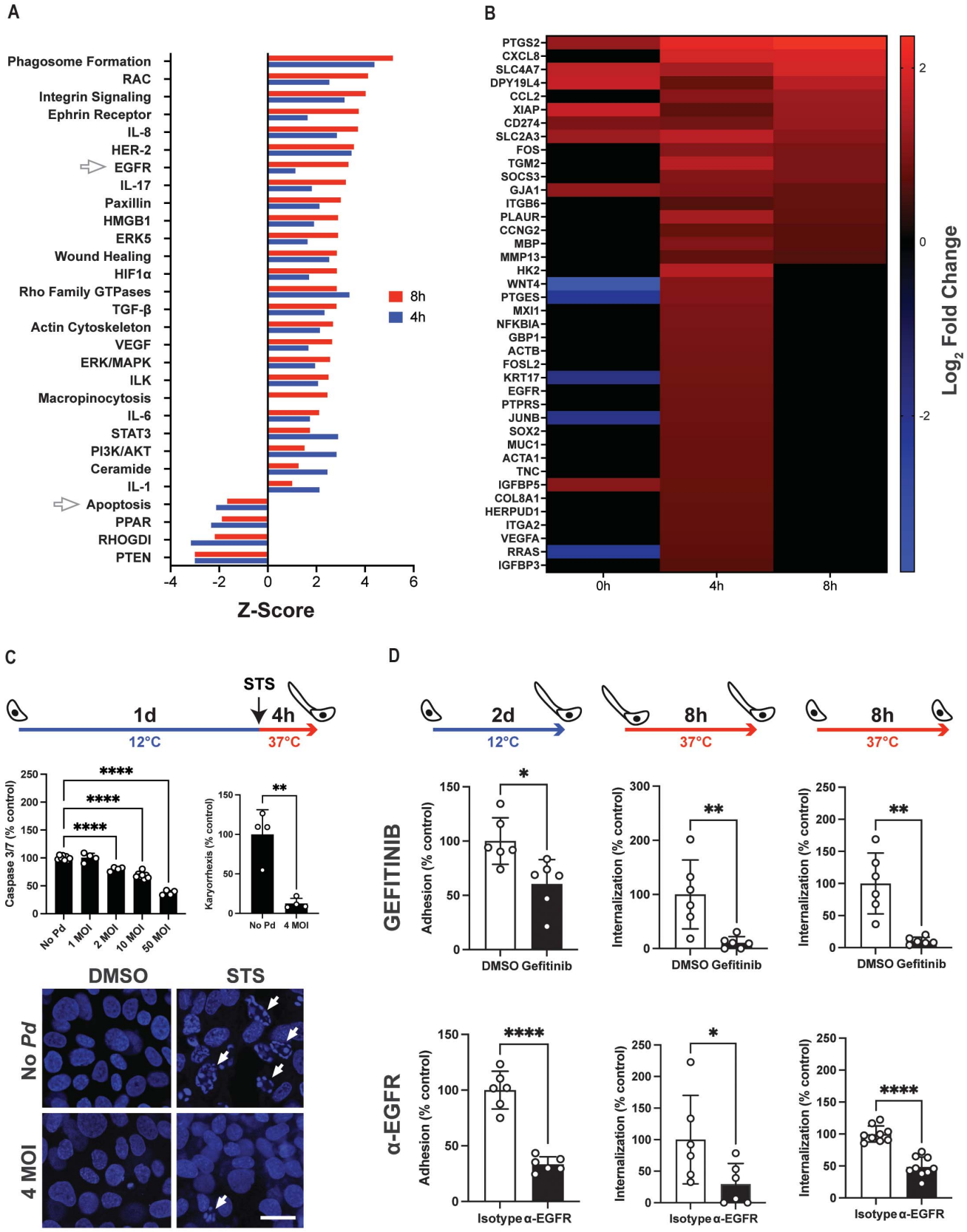

Fig. 3. *P. destructans* blocks apoptosis and enters bat keratinocytes using EGFR. (**A** and **B**) Ingenuity pathway analysis of differentially expressed genes. RNA sequencing was performed on Myluk cells challenged with 10 MOI of live *P. destructans* conidia for two days at 12°C, followed by 0, 4, and 8 hours at 37°C, and compared with unchallenged controls. (A) Pathway enrichment analysis. Predicted directionality (*z* score) of terms identified as enriched for

at least one time point. (B) Relative expression of representative EGFR target genes differentially expressed in at least one time point. Likelihood of a regulatory role of EGFR at 4 hours: $z = 2.408$; $P = 1.24 \times 10^{-19}$. (**C**) Caspase 3 and 7 activity and karyorrhexis (white arrows) in Myluk cells were quantified. Myluk cells were incubated for one day at 12°C with live *P. destructans* conidia and then incubated for 4 hours with 1 μM of the proapoptotic drug staurosporine (STS) or vehicle control at 37°C. ****$P \leq 0.0001$; **$P \leq 0.01$. One-way ANOVA with multiple comparisons correction (caspase 3 and 7 assay) and Student's *t* test (Karyorrhexis assay). Scale bar, 20 μm. (**D**) Role of EGFR in adherence and internalization of *P. destructans* hyphae and conidia. *P. destructans* adherence to and internalization into Myluk keratinocytes was quantified by confocal microscopy. *P. destructans* hyphal and conidial adherence and internalization were measured in the presence of gefitinib (25 μM for 8 hours at 37°C; 12.5 μM for 48 hours at 12°C) or α-EGFR antibody (30 μg/mL) or the vehicle or isotype control, respectively. The antibody is directed against a highly conserved region of EGFR (residues 110 to 322, 87.4% identity with human EGFR). Drug or antibody inhibition was expressed as percentage of control. ****$P \leq 0.0001$; **$P \leq 0.01$; *$P \leq 0.05$. Student's *t* test.

response restricted to the euthermic phase of infection (Fig. 3B and data S1). The cells showed modest up-regulation of proinflammatory chemokines [interleukin-8 (IL8), chemokine ligand 2 (CCL2), and CCL20] without up-regulation of damage-associated cytokines or alarmins (tumor necrosis factor–α, IL1α/β, and IL18) (*32*–*34*), consistent with the nondamaging, stealthy behavior of *P. destructans*. As observed in prior in vivo studies, cyclooxygenase 2 (COX2), an enzyme involved in the conversion of arachidonic acid into proinflammatory eicosanoids (prostaglandin E2 and thromboxane A2), was up-regulated on rewarming (Fig. 3B and data S1) (*12*, *30*, *31*, *35*). However, this up-regulation at the transcript level did not translate into eicosanoid production measured by gas chromatography–tandem mass spectrometry or enzyme-linked immunosorbent assay (fig. S7). This discordance may stem from the lack of cell membrane damage–induced Ca^{2+} flux necessary for phospholipase A2 activation and arachidonic acid synthesis (*36*).

Blocking apoptosis enhances P. destructans colonization

Apoptosis-induced clearance of infected cells can block microbial progression through infected tissues such as skin (*19*). To counteract this host response, *C. albicans* and *A. fumigatus* inhibit apoptosis of invaded cells to favor intracellular survival and dissemination (*19*). The repression of the apoptosis pathways uncovered by our transcriptomic analysis was consistent with our in vivo and in vitro observations and the absence of *P. destructans*–induced cell death. Hence, we hypothesized that *P. destructans* inhibits apoptosis of infected keratinocytes. To test this idea, we challenged Myluk cells with live *P. destructans* conidia for 1 day at 12°C, then exposed them to the proapoptotic drug staurosporine for 4 hours at 37°C. We then quantified both caspase 3 and 7 activity and karyorrhexis (Fig. 3C). Addition of *P. destructans* blunted drug-induced apoptosis of Myluk in a dose-dependent manner. By contrast, challenging the keratinocytes under similar conditions but with heat-killed germinated conidia or conditioned media did not reduce staurosporine-induced caspase 3 or 7 activity (fig. S8). Thus, viable *P. destructans* inhibits apoptosis of keratinocytes by direct contact independently of secreted factors. The upstream pathways that *P. destructans* modulates to block activation of effector caspases 3 and 7 are unknown. *A. fumigatus* and *C. albicans* block cell death of epithelial cells by up-regulating the prosurvival pathway, phosphatidylinositol-3,4,5-trisphosphate–protein kinase B (PI3K–Akt) (*19*). *P. destructans* infection of keratinocytes likewise activates this pathway while repressing the phosphatase and tensin homolog pathway that negatively regulates intracellular levels of PI3K (Fig. 3A) (*37*).

Role of EGFR in P. destructans entry into keratinocytes

Our RNA sequencing data point to a role for EGFR during *P. destructans* interaction with keratinocytes (Fig. 3, A and B). Furthermore, immunolabeling of EGFR in *P. destructans*–infected Myluk cells showed colocalization of this receptor with the fungus (fig. S9). EGFR is a transmembrane tyrosine kinase receptor that mediates adhesion and actin-mediated endocytosis of *C. albicans* and *Rhizopus oryzae* by epithelial cells (*38*–*41*). We hypothesized that EGFR could facilitate *P. destructans* adhesion to keratinocytes and hyphal- and conidia-induced endocytosis at 37°C but not (actin-independent) hyphal penetration at 12°C. To test this, we used two approaches. Firstly, we blocked EGFR kinase activity with a Food and Drug Administration–approved small molecule, gefitinib (Fig. 3D and figs. S10A and S11). Notably, EGFR tyrosine kinase remains active above 4°C and is able to be inhibited even when keratinocytes are incubated at 12°C (*42*). Secondly, we neutralized the extracellular domains of EGFR with antibodies (Fig. 3D and figs. S10B and S11). At 37°C, gefitinib treatment and antibody blockade each diminished endocytic internalization of hyphae and conidia (Fig. 3D). At 12°C, both treatments also reduced adherence of *P. destructans* hyphae to Myluk cells (Fig. 3D). Both gefitinib and anti-EGFR antibody exerted concentration-dependent effects (figs. S10A and S10B). Neither treatment affected the adhesion of hyphae or conidia to Myluk cells at 37°C (fig. S11). As a control, we showed that neither gefitinib nor antibody impaired cell viability (fig. S10C). Thus, EGFR promotes the binding of actively growing *P. destructans* hyphae to the host cell at 12°C and mediates internalization of both hyphae and conidia at 37°C. Gefitinib and anti-EGFR antibody retard these events.

These results indicate that EGFR is required for entry of *P. destructans* into bat keratinocytes. In models of oral candidiasis, EGFR is activated by binding *Candida* surface ligands (Als3 and Ssa1) or endogenous plasma membrane–bound ligands liberated through metalloproteinases (*38*, *43*). *P. destructans* expresses a Ssa1 ortholog (VC83_01046, 97.6% identity) (fig. S5). Likewise, EGFR endogenous ligands, such as EGF-like growth factor and epiregulin, together with their cleaving ADAM metalloproteinases (ADAM8, ADAM10, and ADAMTS1), are up-regulated in our studies and in prior in vivo transcriptomic studies (data S1) (*31*). Alternatively, other transmembrane receptors can dimerize or form transmembrane clusters with EGFR to induce its activation. Integrin, HER2, and ephrin receptor pathways were found to be activated in our transcriptomic studies (Fig. 3A). These receptors, in combination with EGFR, recognize and internalize *C. albicans* and *Rhizopus* spp. and may partner with EGFR in recognition of *P. destructans* (*38*, *41*, *44*, *45*). EGFR might also be activated by cytosolic receptors that confer intracellular receptor phosphorylation. Our RNA sequencing data showed that activation of the cytosolic aryl hydrocarbon receptor (AHR) pathway, essential in EGFR-mediated response to *C. albicans* by epithelial cells, occurred in Myluk cells, as evidenced by the up-regulation of the AHR agonists, metabolizing enzymes CYP1A1 and CY1B1 (data S1) (*46*, *47*).

Discussion

We have developed a cell culture model of torpor and arousal using little brown bat keratinocytes and observed infection by the fungal pathogen *P. destructans* at these different stages of bat life history. We showed that *P. destructans* inhibits apoptosis of infected keratinocytes and enters and spreads through these cells by two EGFR-dependent mechanisms: active hyphal penetration during torpor and induced hyphal and conidial endocytosis during arousal. Furthermore, we demonstrated that conidial DHN-melanin interrupts endolysosomal maturation, facilitating intracellular survival during arousals and enabling germination on return to torpor. We capitalized on EGFR-mediated mechanisms

of host–*P. destructans* interaction to show that treatment with gefitinib or anti-EGFR antibody reduced *P. destructans* invasion of bat keratinocytes. Our findings offer new insight into the mechanisms of WNS pathogenesis and warrant further validation with more complex in vitro and in vivo models.

P. destructans adapts its invasive strategy to the host hibernation status. It enters bat keratinocytes by active hyphal penetration during the cold phase of the infection, when host cell actin polymerization is limited and endocytic uptake is idle (*48*, *49*). Conversely, during the warm phase, both *P. destructans* hyphae and conidia are internalized by keratinocytes in an actin-dependent manner. This plasticity of *P. destructans* allows the fungus to remain infective during fungal growth–conducive (bat torpor) and –restrictive (bat arousal) phases of hibernation (*11*). Once *P. destructans* conidia are internalized, DHN-melanin in the conidia protects them from endolysosomal killing. Conidia-containing endosomes that fail to fuse with lysosomes and mature might provide intracellular reservoirs inaccessible to host antifungal immune response during arousals (*12*). Germination of internalized conidia and progression into neighboring keratinocytes upon return to 12°C could promote pervasion of the epidermis once conditions are favorable for this psychrophilic fungus.

Treatment with gefitinib has been shown to rescue mice from experimental oral candidiasis and pulmonary mucormycosis (*38*, *40*), and it may offer a drug lead for bat WNS. This intervention stems from recognition that EGFR mediates adhesion and internalization of *C. albicans* and *Rhizopus* spp. into oral and lung epithelium, respectively (*38*, *40*, *41*, *44*), as it does for *P. destructans* in bat keratinocytes.

REFERENCES AND NOTES

1. T. H. Kunz, E. Braun de Torrez, D. Bauer, T. Lobova, T. H. Fleming, *Ann. N. Y. Acad. Sci.* **1223**, 1–38 (2011).
2. J. G. Boyles, P. M. Cryan, G. F. McCracken, T. H. Kunz, *Science* **332**, 41–42 (2011).
3. T. L. Cheng *et al.*, *Conserv. Biol.* **35**, 1586–1597 (2021).
4. W. F. Frick *et al.*, *Science* **329**, 679–682 (2010).
5. J. R. Hoyt, A. M. Kilpatrick, K. E. Langwig, *Nat. Rev. Microbiol.* **19**, 196–210 (2021).
6. D. S. Blehert *et al.*, *Science* **323**, 227 (2009).
7. S. Solari, Myotis lucifugus (amended version of 2018 assessment), *The IUCN Red List of Threatened Species* (2021), vol. e.T14176A208031565. doi:10.2305/IUCN.UK.2021-3.RLTS.T14176A208031565.en
8. J. M. Lorch *et al.*, *Nature* **480**, 376–378 (2011).
9. A. N. Makanya, J. P. Mortola, *J. Anat.* **211**, 687–697 (2007).
10. M. Choi, C. Lee, *Biomol. Ther. (Seoul)* **23**, 391–399 (2015).
11. M. L. Verant, J. G. Boyles, W. Waldrep Jr., G. Wibbelt, D. S. Blehert, *PLOS ONE* **7**, e46280 (2012).
12. K. A. Field *et al.*, *Mol. Ecol.* **27**, 3727–3743 (2018).
13. J. Ou *et al.*, *Cell* **173**, 851–863.e16 (2018).
14. K. A. Jonasson, C. K. R. Willis, *J. Exp. Biol.* **215**, 2141–2149 (2012).
15. W. Fei, Y. Liu, *Appl. Biochem. Biotechnol.* **195**, 1–16 (2023).
16. C. U. Meteyer, J. Y. Dutheil, M. K. Keel, J. G. Boyles, E. H. Stukenbrock, *Virulence* **13**, 1020–1031 (2022).
17. C. Seidel *et al.*, *Front. Microbiol.* **11**, 1955 (2020).
18. J. Lachat *et al.*, *Nat. Commun.* **13**, 3781 (2022).
19. G. Camilli, M. Blagojevic, J. R. Naglik, J. P. Richardson, *Trends Cell Biol.* **31**, 179–196 (2021).
20. D. C. Sheppard, S. G. Filler, *Cold Spring Harb. Perspect. Med.* **5**, a019687 (2014).
21. A. Håkansson, C. C. Bentley, E. A. Shakhnovic, M. R. Wessels, *Proc. Natl. Acad. Sci. U.S.A.* **102**, 5192–5197 (2005).
22. K. Wolff, K. Konrad, *J. Ultrastruct. Res.* **39**, 262–280 (1972).
23. S. Sayedyahossein *et al.*, *FASEB J.* **29**, 711–723 (2015).
24. T. Akoumianaki *et al.*, *Cell Host Microbe* **19**, 79–90 (2016).
25. I. Kyrmizi *et al.*, *Nat. Microbiol.* **3**, 791–803 (2018).
26. A. Thywißen *et al.*, *Front. Microbiol.* **2**, 96 (2011).
27. M. Pihet *et al.*, *BMC Microbiol.* **9**, 177 (2009).
28. S. Kumari, S. Mg, S. Mayor, *Cell Res.* **20**, 256–275 (2010).
29. A. N. Atre *et al.*, *FEMS Immunol. Med. Microbiol.* **55**, 74–84 (2009).
30. C. M. Davy *et al.*, *Virulence* **11**, 781–794 (2020).
31. K. A. Field *et al.*, *PLOS Pathog.* **11**, e1005168 (2015).
32. T. Hasegawa, T. Oka, S. Demehri, *Front. Immunol.* **13**, 876515 (2022).
33. D. Yang, Z. Han, J. J. Oppenheim, *Immunol. Rev.* **280**, 41–56 (2017).
34. F. Pinci *et al.*, *Front. Immunol.* **13**, 1074440 (2022).
35. E. A. Dennis, P. C. Norris, *Nat. Rev. Immunol.* **15**, 511–523 (2015).
36. C. C. Leslie, *J. Biol. Chem.* **272**, 16709–16712 (1997).
37. A. Carracedo, P. P. Pandolfi, *Oncogene* **27**, 5527–5541 (2008).
38. W. Zhu *et al.*, *Proc. Natl. Acad. Sci. U.S.A.* **109**, 14194–14199 (2012).
39. R. Roskoski Jr., *Pharmacol. Res.* **79**, 34–74 (2014).
40. T. N. Watkins *et al.*, *mBio* **9**, e01384–e18 (2018).
41. M. Swidergall *et al.*, *PLOS Pathog.* **17**, e1009221 (2021).
42. R. Campos-González, J. R. Glenney Jr., *Cell Regul.* **2**, 663–673 (1991).
43. J. Ho *et al.*, *Nat. Commun.* **10**, 2297 (2019).
44. M. Swidergall, N. V. Solis, M. S. Lionakis, S. G. Filler, *Nat. Microbiol.* **3**, 53–61 (2018).
45. A. Alqarihi *et al.*, *mBio* **11**, e01087–e20 (2020).
46. E. Buommino *et al.*, *Med. Mycol.* **56**, 987–993 (2018).
47. N. V. Solis, M. Swidergall, V. M. Bruno, S. L. Gaffen, S. G. Filler, *mBio* **8**, e00025–e17 (2017).
48. S. C. Silverstein, R. M. Steinman, Z. A. Cohn, *Annu. Rev. Biochem.* **46**, 669–722 (1977).
49. G. Li, J. K. Moore, *Mol. Biol. Cell* **31**, 1154–1166 (2020).

ACKNOWLEDGMENTS

We thank the US Geological Survey (USGS) National Wildlife Health Center (NWHC) for providing the little brown bat skin samples to generate the Myluk cell line and conduct in vivo EM studies as well as the bat skin histological preparation for bright field microscopy. We are particularly thankful to T. Rocke for her assistance in acquiring funding from USGS and the National Science Foundation (NSF) and to D. Blehert and J. Lorch for presubmission review of the manuscript. We also thank the Lambert Lab at University of Wisconsin (UW)–Madison and especially D. Lee for providing lentiviral particles and advise in keratinocyte culture, isolation, and immortalization; the Cellular and Molecular Neuroscience (CMN) Core at Waisman Center UW Madison and K. M. Knobel for support with Imaris processing of confocal images and capturing of histological photographs of bat skin; the Sauer Lab at UW Madison, particularly Z. Morrow for performing eicosanoid MS and ELISAs; the Electron Microscope Core (SMPH) and Nett Lab at UW Madison with special appreciation to R. Massey and C. Johnson for their support with electron microscopy sample preparation and scoping; the University of Wisconsin Biotechnology Center (UWBC) Gene Expression Center and Bioinformatics Resource Center for Next-Generation Sequencing and Analysis; the Klein Lab members L. Dos Santos Dias, S. L. Lichtenberger, P. Thakur, and J. Y. Chen for their technical support with Western blotting (L.D.S.D.), flow cytometry (S.L.L.), microscopy (P.T.) and cell culture (J.Y.C.); and S. Fites for presubmission review of the manuscript. **Funding:** The U.S. Geological Survey grant G20AC00050 (B.S.K.); The US Fish and Wildlife Service 13190304 (B.S.K.); The Canadian Institute for Advanced Research MSN247980 (B.S.K.); The National Science Foundation 2301729 (B.S.K.); La Caixa Foundation fellowship (ID 100010434) under agreement LCF/BQ/AA17/11610020 (M.I.-A.); Comparative Biomedical Sciences Training Grant T32OD010423 funded by the National Institutes of Health (M.I.-A.); Morris Animal Foundation D23ZO-461 fellowship training grant (M.I.-A.). **Author contributions:** Conceptualization: M.I.-A. and B.S.K.; Methodology: M.I.-A. and B.S.K.; Investigation: M.I.-A.; Visualization: M.I.-A.; Funding acquisition: M.I.-A. and B.S.K.; Project administration: B.S.K.; Supervision: B.S.K.; Writing – original draft: M.I.-A.; Writing – review and editing: M.I.-A. and B.S.K. **Competing interests:** The authors declare no competing interests. **Data and materials availability:** All data are available in the main text or supplementary materials.

SUPPLEMENTARY MATERIALS

science.org/doi/10.1126/science.adn5606
Materials and Methods
Figs. S1 to S11
References (*50*–*70*)
MDAR Reproducibility Checklist
Data S1 and S2

Submitted 15 December 2023; accepted 14 May 2024
10.1126/science.adn5606